Generation of multi-terawatt vortex laser beams

Craig Ament,[1] Lee Johnson,[1] Andreas Schmitt-Sody,[2]
Adrian Lucero,[2] Thomas Milster,[1] and Pavel Polynkin[1,*]

[1] *College of Optical Sciences, The University of Arizona, Tucson, Arizona 85721, USA*

[2] *Air Force Research Labs, Kirtland Air Force Base, Albuquerque, New Mexico 87117, USA*

arXiv:1402.7069v1 [physics.optics] 27 Feb 2014

Abstract

We report the fabrication of large-area phase masks on thin fused-silica substrates that are suitable for shaping multi-terawatt femtosecond laser beams. We apply these phase masks for the generation of intense femtosecond optical vortices. We further quantify distortions of the vortex beam patterns that result from several common types of mask defects.

* Corresponding author: ppolynkin@optics.arizona.edu

I. INTRODUCTION

Laser beam shaping is a concept as old as the laser itself and is essential in such diverse applications of the laser as material processing, lithography and biology. Recently, laser beam shaping has been applied to the studies of self-action effects of ultra-intense femtosecond laser pulses in air. Phase and amplitude perturbations across the shaped beam profile act as nucleation sites that determine the placement of intense filaments resulting from self-focusing of the beam [1]. Various complex beam shapes have been applied to filamentation studies in air including fundamental Bessel beams [2–4], Airy beams [5] and optical vortices [6, 7]. Propagation dynamics of intense optical vortices in air is particularly interesting. It has been argued that the bottle-like distributions of dilute plasma filaments that are created in air through self-focusing of such beams can act as extended conduits for microwave radiation [8, 9].

Airy and vortex laser beam patterns investigated in [5, 7] have been produced through the modulation of initially smooth input beam profiles with specially designed transmissive phase masks. Those masks have been made by profiling thin polyamide coatings atop fused silica substrates. They have an estimated damage threshold of the order of $10\,\mathrm{mJ/cm^2}$, for laser pulses with about 40 fs duration. For the centimeter-scale input laser beam diameter, the above damage threshold corresponds to the maximum pulse energy of the order of 10 mJ. Such pulse energies are adequate for laboratory-scale investigations with the meter-scale extent of the generated plasma filaments. For real outdoor applications that require filament lengths of tens to hundreds of meters, the input pulse energy has to be scaled to hundreds of mJ and beyond. In that case polyimide phase masks become inadequate as they are easily damaged by the laser beam on a single laser shot. The application of either purely reflective phase masks or transmissive masks made of an optical material with high damage threshold is necessary.

In this paper, we report the fabrication of phase masks with area of up to $50\,\mathrm{mm} \times 50\,\mathrm{mm}$ made on 0.5 mm-thick fused silica substrates. We have experimentally confirmed that these masks withstand an extended exposure to femtosecond laser beams with energy per pulse of up to 230 mJ. We argue that the damage threshold for these masks is, in fact, higher than that and should not be significantly lower than ablation threshold of fused silica, which is of the order of $1\,\mathrm{J/cm^2}$ for femtosecond laser pulses. We apply our phase masks for the

generation of intense vortex beams and investigate distortions in the vortex beam patterns that result from several common types of mask defects.

To the best of our knowledge, the highest previously reported peak intensity of a femtosecond optical vortex beam, that has been experimentally generated, is about 200 GW [7]. We here report the generation of intense femtosecond vortex beams of various orders with the maximum peak intensity of about 4.6 TW. We show that self-focusing of such beams in air results in the generation of meter-long ring patterns of multiple ($\sim$30) plasma filaments.

II. MASK FABRICATION

The fabrication of large-area fused-silica phase masks involves two major steps. In the first step, the desired grayscale phase pattern is lithographically imprinted into a several micron-thick layer of polyimide photoresist atop a fused silica substrate, using a Mask-less Lithography Tool (MLT). MLT makes use of a unidirectional raster stage and a scanning polygonal mirror which directs an externally modulated Argon-Ion Innova Sabre Laser by Coherent, Inc. operating at the wavelength of 355 nm and generating output power variable from 100mW to 1.2W. The resist exposure level is tailored by adjusting the laser output power as well as the number of exposure steps and the development time, in order to reach the desired depth in the photoresist. Phase patterns imprinted into photoresist are profiled with a Veeco NT9800 Optical Profiling System.

In the second fabrication step, illustrated in Figure 1, the pattern is transferred from the polyimide photoresist to the fused silica substrate via reactive ion etching (RIE). The gas mixture used in the RIE process consists of O_2, Ar, and CHF_3 gases with flow rates of 2.8 standard cubic centimeters (sccm), 4 sscm, and 34 sscm, respectively. The RF power used in RIE is 300 watts, while the pressure in the etch chamber is maintained at 50 mTorr. No adverse effects such as boiling of photoresist were observed under these etching conditions.

Phase patterns on all masks that we fabricate are defined modulo 2π, meaning that whenever the local phase ramp across the surface of the mask reaches the value of 2π, it is reset to zero. The rates at which RIE removes photoresist and fused silica are somewhat different. This difference in etching rates depends on the formulation of the resist, as well as on the exact composition and flow rates of gases used in RIE. In our particular case, the etching rates for resist and fused silica differed by about 25%. Therefore, in order to achieve

the target phase contrast on the final fused-silica mask, the mask on the photoresist had to be made 25% thicker than the target depth of the mask on fused silica.

III. GENERATION OF INTENSE FEMTOSECOND VORTEX LASER BEAMS

The specific beam shapes that we generated using our fused-silica masks are optical vortices of various orders. An optical vortex beam is generated from a flat-top or a Gaussian beam through the application of phase-only beam modulation in the form:

$$\Phi(r, \theta) \; = \; im\theta \, , \tag{1}$$

followed by either propagation into far field or focusing the beam with a lens or a curved mirror [10]. In the above formula, Φ is a variable phase that is applied to the transverse amplitude distribution of the beam by the phase mask, (r, θ) are polar coordinates, and m is the order of the vortex. The resulting intensity pattern of the vortex beam, either in far field or in the focal plane of a focusing optic, looks like a doughnut. The diameter of the intensity doughnut grows approximately linearly with the order of vorticity m.

Although our mask fabrication process allows us to generate vortex beams of arbitrary order, we here limit our consideration to the cases of vortices of orders 3 and 8. The phase profiles of the corresponding masks, defined modulo 2π, together with the corresponding

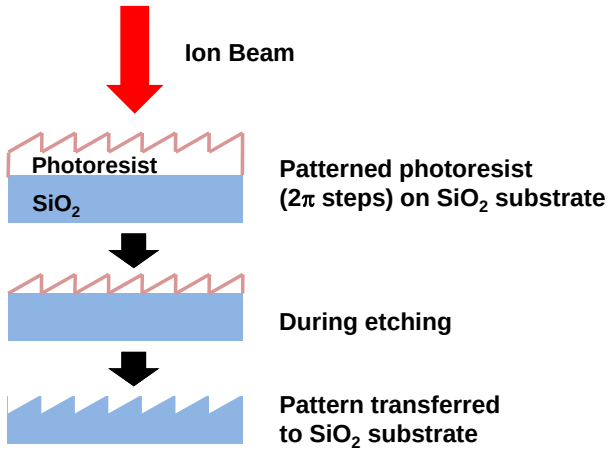

FIG. 1. Illustration of the second step of the masks fabrication process. The desired grayscale phase pattern, imprinted into a several micrometer-thin layer of photoresist atop a fused-silica substrate, is etched into the substrate via reactive ion etching.

intensity distributions that have been numerically computed and therefore are ideal (free of any defects or imperfections), are shown in Figure 2.

In real life, neither the phase masks nor the input laser beam are ideal. Various phase defects that result from the imperfections inherent to the mask fabrication process, as well as spurious amplitude and phase modulations of the input beam translate into deviations of the generated vortex beam patterns from their ideal unperturbed shapes such as the ones shown in Figure 2. Specifically, the peak intensity of the non-ideal vortex ring will be not uniform but will undulate along the circumference of the ring and the intensity on the beam axis will be different from zero, as would be the case for an ideal optical vortex. For ultra-intense vortex laser beams, imperfections of the beam pattern may result in the premature azimuthal collapse of the beam and in its fragmentation into multiple individual filaments that populate the doughnut intensity feature. Such azimuthal mode of collapse may precede the self-similar collapse of the intensity ring, as reported in [7]. The azimuthal fragmentation of the vortex intensity ring is not a necessarily undesirable effect in practice, as it results in the deterministic placement of intense laser filaments on the ring. In that case, the resulting bottle-like distribution of plasma filaments will not fluctuate from one laser shot to another, which, in fact, may be beneficial in some applications.

In the top part of Figure 3, we show the intensity patterns of experimentally generated optical vortices of orders 3 and 8. In order to generate these beam shapes, the input laser

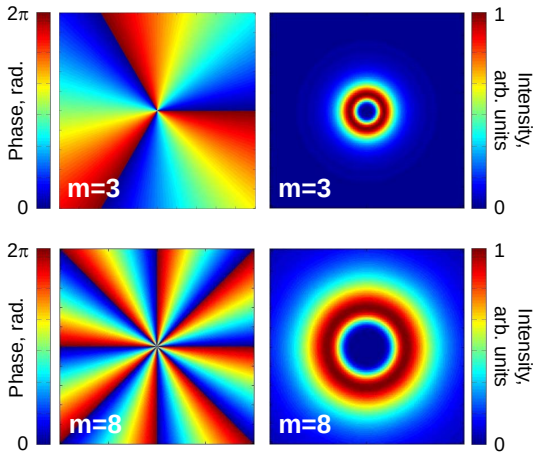

FIG. 2. Examples of numerically simulated ideal vortex beam patterns of orders 3 and 8. The phase profiles, defined modulo 2π, are shown in the left panels, with the corresponding transverse beam intensity distributions shown in the right panels.

beam from a Ti:Sapphire laser oscillator was telescoped to the beam diameter of 5 mm, passed through the appropriate phase mask fabricated according to the process described above and focused with a lens with a focal length equal to 1 meter. The laser was attenuated to ensure linear propagation through the phase masks and focusing optics, as well as through the entire optical path in the air. Thus generated vortex beam patterns were photographed in the focal place of the lens with a CCD camera sensitive to 800 nm light, which is the center wavelength of the laser source. The deviations of the beam patterns from ideal vortex beams are evident for both examples shown. Specifically, the on-axis intensity is not identically zero, which is especially evident for the case of the 8^{th} order vortex. Furthermore, the intensity of the doughnut feature is not uniform along its circumference. The imperfections in the phase masks that may have caused these beam distortions are discussed in detail in the following sections of the paper.

In the bottom part of Figure 3, we show the ring patterns of multiple plasma filaments

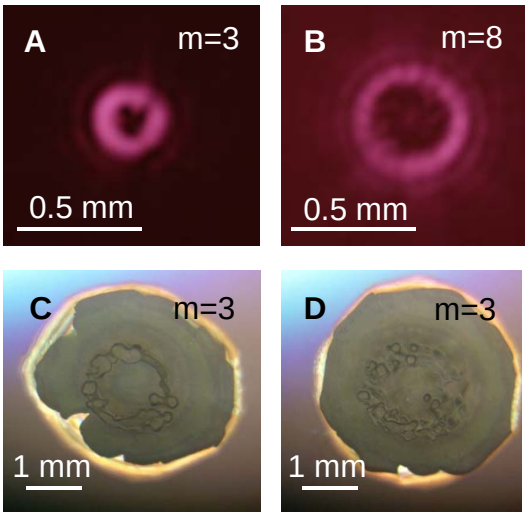

FIG. 3. (A,B) Intensity distributions of vortex beams of orders 3 and 8 in the linear propagation regime (at low intensity). The $1/e^2$ E-field radius of the Gaussian beam incident on the masks equals 5 mm, and the focal length of the focusing lens used is 1 m. Distortions of the doughnut-shaped beam intensity patterns are evident. (C,D) Bottle-like distributions of plasma filaments produced through self-focusing of an intense optical vortex of order 3 in air. Focusing conditions are specified in the text. The energy of the 50 fs-long laser pulse is 150 mJ (C) and 230 mJ (D), corresponding to the highest peak laser power of 4.6 TW.

that resulted from self-focusing of an intense femtosecond vortex beam of order 3 in air, at two different levels of optical power. The laser source used to produce these filament patterns is a multi-Terawatt Ti:Sapphire laser system that generates 50 fs-long pulses at a rate of ten pulses per second. At the time when these experiments were conducted, the maximum attainable compressed pulse energy was about 230 mJ, corresponding to the peak laser power of about 4.6 Terawatt. The output beam diameter from the laser is 3 cm. The beam is converted into an optical vortex of order 3 through the application of a 50 mm-diameter fused silica vortex phase mask with the thickness of 0.5 mm, followed by beam focusing with a curved mirror with the focal length of 5 m. No optical damage of the mask was noticed after a continuous extended exposure to multiple laser shots, up to the maximum pulse energy of 230 mJ. At that point the peak fluence and intensity of the laser beam incident on the phase mask were 33 mJ/cm^2 and 0.65 TW/cm^2, respectively. There is no apparent reason for the damage threshold of these masks to be be significantly different from the laser ablation threshold of fused silica, which, for $\sim$50 fs-long laser pulses at 800 nm wavelength, is of the order of 1 J/cm^2 [11].

As the intense vortex laser beam propagates in air, beam self-focusing leads to the generation of multiple plasma filaments that are evident in the images of single-shot burns made by the beam on the front surface of a computer CD, shown in the bottom part of Figure 3. The broad and approximately round gray area evident in the images results from the blown-off foil on the back side of the CD. The number of plasma filaments grows as the laser pulse energy is increased. In the two particular cases shown in Figures 3 (A) and (D), the laser pulse energy is 150 mJ and 230 mJ, respectively. The filament patterns shown are imaged at 60 cm before the focal plane of the focusing optic. Closer to the focal plane, the filament pattern becomes severely distorted and does not look like a ring anymore. At the highest pulse-energy level of 230 mJ, the number of plasma filaments populating the doughnut-shaped intensity feature of the beam is about 30.

IV. DISTORTIONS OF VORTEX PATTERNS RESULTING FROM COMMON TYPES OF MASK DEFECTS

In what follows, we will discuss common types of imperfections that occur in the fabrication process of vortex phase masks. Through numerical simulations, we will quantify errors

in the vortex beam patterns that result from these imperfections. Our simulations assume linear propagation of the beam and are based on the straightforward numerical calculation of the Fresnel diffraction integral. In all cases shown, the beam incident of the phase mask is assumed to be Gaussian with the $1/e^2$ E-field radius of 5 mm, at 800 nm wavelength. Immediately following the mask, the beam is focused by a focusing optic with the focal length of 1 meter.

In practice, the acceptable modulation of the vortex intensity pattern will depend on the particular application of the vortex beam. Our results will set quantitative limits on common-type imperfections of the phase mask, used to generate the beam, at a given maximum acceptable beam distortion.

A. Error in 2π Phase Step

As we pointed out above, phase patterns on all phase masks that we fabricate are defined modulo 2π. Whenever the phase ramp across the surface of the mask reaches 2π, the phase is reset to zero. Phase modulation imposed on the beam by the mask, at a particular point on the mask, is proportional to the mask thickness at that point and inversely proportional to the beam wavelength. Therefore, if the thickness contrast on the fabricated mask deviates from the target value, the value of the maximum phase modulation by the mask will be

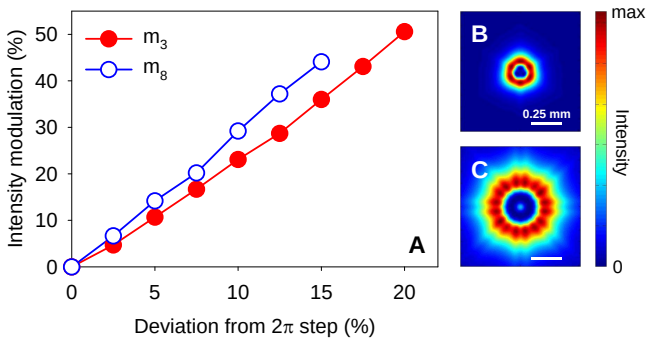

FIG. 4. (A) Peak-to-peak intensity modulation of the doughnut intensity feature of the beam as a function of the % error in the maximum phase step of the phase mask, for continuous-wave optical vortices of orders 3 and 8. (B) Beam intensity pattern in the focal plane of the focusing optic, for an optical vortex of order 3 and for 5% error in the maximum phase step. (C) Same for a vortex of order 8.

different from 2π. The same effect will result if the mask is used to modulate a laser beam having a different wavelength from the one it is designed for.

In Figure 4 (B,C), we show two examples of imperfect vortex beam patterns that result from the deviation of the maximum phase contrast by 5% from the target value of 2π. In the Figure 4(A), we show the resulting azimuthal modulation of the ring intensity pattern, as a function of the % error in the maximum phase contrast of the phase mask used to generate the beam. The intensity modulation of the ring is defined as the maximum relative peak-to-peak variation of intensity along the circumference of the intensity doughnut. As evident from these simulations, the modulation of the ring intensity pattern grows approximately linearly with the % error in the maximum phase contrast of the phase mask. The beam distortion is somewhat higher for larger vortex orders. In addition to the modulation of the ring intensity feature, imperfect higher-order vortices exhibit pronounced on-axis intensity.

B. Effect of Broad Spectrum of Light

The second type of distortion of optical vortex beams that we consider results from the finite optical bandwidth of the incident laser beam. Even a perfectly fabricated mask will be ideal only for one optical wavelength in the spectrum of the laser. In the calculation of the beam distortion in this case, we compute the spatial distribution of the beam fluence (intensity integrated over pulse duration), in the focal plane of the focusing optic.

The result of the calculation is shown in Figure 5. As evident from the data, the ring

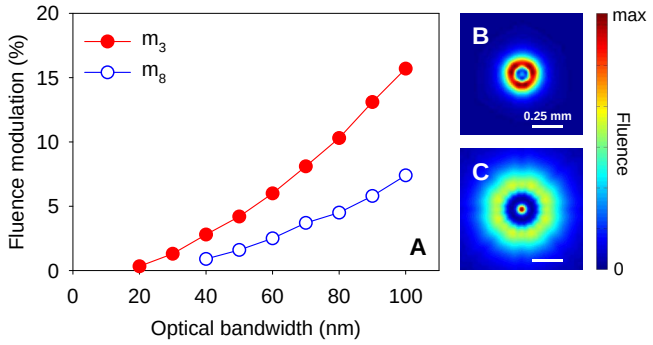

FIG. 5. (A) Peak-to-peak fluence modulation of the vortex ring as a function of the optical bandwidth of the laser beam. (B) Fluence pattern for an optical vortex of order 3 and for optical bandwidth equal to 100 nm. (C) Same for a vortex of order 8.

modulation for higher-order vortices is, in fact, smaller than that for lower-order vortices. This trend results from averaging of errors for different spectral components of the beam that becomes more effective as the order of vorticity is increased. We point out that for higher-order vortices, the emergence of significant intensity on the beam axis becomes the dominant type of error for the case of pulsed laser beams with large optical bandwidth.

The typical value of optical bandwidth for amplified Ti:Sapphire laser chains is about 30 nm, in which case the modulation of the vortex ring patterns caused by the finite bandwidth of the laser source is of the order of one percent or lower.

C. Circular Defect

Another type of defect that is common in mask fabrication is a point or circular defect. The effect of this type of defect on the generated vortex beam pattern will depend on the

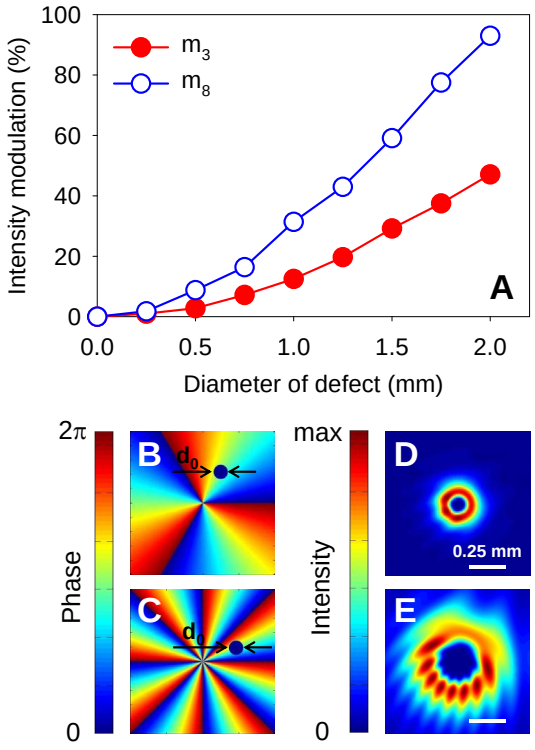

FIG. 6. (A) Peak-to-peak intensity modulation of the vortex ring as a function of the diameter of the circular defect on the phase mask. (B,C) Illustrations of the location of the circular defect on vortex phase masks of orders 3 and 8. (D,E) Corresponding beam patterns for the particular diameter of the circular defect equal to 1 mm.

location and size of the defect. To get an idea about severity of the vortex beam distortion resulting from this type of defect, we assume that the defect is located at a median of the 2π phase ramp on the mask, and its center is one $1/e^2$ beam radius away from the center of the mask. We model the defect as uniform zero phase inside a circle of a particular diameter d_0, as illustrated in Figures 6(B,C) for vortex masks of orders 3 and 8, respectively. The calculation in this case is performed for an otherwise ideal phase mask and for a continuous-wave laser beam.

As follows from the results of the calculation, the modulation of the ring intensity pattern grows approximately quadratically with the diameter of the defect, which corresponds to the approximately linear growth with the area of the defect. For the same defect size, beam distortion is more severe for larger vortex orders.

D. Line Defect

The last defect type we consider is the line defect. This defect type will result, for example, from stitching of several independently fabricated phase masks into a single large-area mask. As in the case of the circular defect, the appearance and severity of beam distortion in this case will depend on the size of the defect and on its location on the mask. To be specific, we assume that the defect is perpendicular to one of the 2π phase-reset lines and is located one $1/e^2$ beam radius away from the center of the mask, as illustrated in Figures 7(B,C), for vortex orders 3 and 8. As in the case of a circular defect, we model line defect as uniform zero phase inside a rectangular area of a particular width d_0 spanning the entire length of the mask.

The results of the calculation for this case are shown in Figure 7. Intensity modulation of the doughnut intensity feature grows approximately linearly with the width of the line defect, and the effect of this type of defect is more severe for vortices of higher order.

V. CONCLUSION

In conclusion, we have reported experimental results on the fabrication and application of large-area, grayscale phase masks suitable for beam shaping of femtosecond laser systems with multi-Terawatt peak power. We have applied these masks for the generation of intense

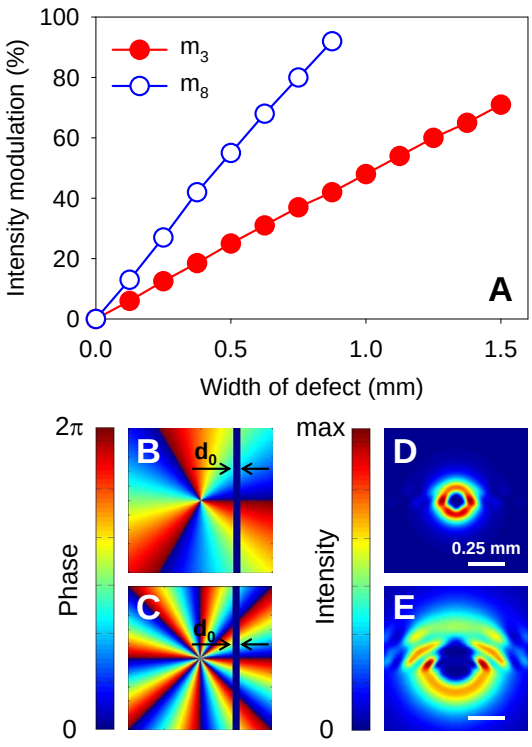

FIG. 7. (A) Peak-to-peak intensity modulation of the vortex ring as a function of the width of the line defect on the phase mask. (B,C) Illustrations of the location of the linear defect on vortex phase masks of orders 3 and 8. (D,E) Corresponding beam patterns for the particular width of the linear defect equal to 0.5 mm.

optical vortices of various orders, with peak power of up to 4.6 TW. The corresponding maximum peak intensity of the laser beam incident on the surface of the masks was 0.65 TW/cm^2. The pulse energy of optical vortex beams generated in our experiments is by more than one order of magnitude higher than what was reported previously. The peak intensity of vortex beams in our experiments was sufficient for the generation of meter-long bottle-shaped patterns of multiple plasma filaments in ambient air. Through numerical simulations, we have analyzed distortions of the generated vortex beam patterns that result from common types of mask defects. Our simulation results will be useful for estimations of maximum acceptable mask imperfections for a given level of modulation of vortex beam patterns.

This work was supported by The United States Air Force Office of Scientific Research (U.S. AFOSR) under Grants No. FA9550-12-1-0143, No. FA9550-12-1-0482, and No. FA9550-10-1-0561 and by The United States Defense Threat Reduction Agency (DTRA)

under Grant No. HDTRA1-14-1-0009. Craig Ament acknowledges the support from the Graduate Scholarship by the Directed Energy Professional Society (DEPS).

---

[1] G. Mechain, A. Couairon, M. Franco, B. Prade, A. Mysyrowicz, "Organizing multiple femtosecond filaments in air", Phys. Rev. Lett. **93**, 035003 (2004).

[2] P. Polynkin, M. Kolesik, A. Roberts, D. Faccio, P. Di Trapani, J. Moloney, "Generation of extended plasma channels in air using femtosecond Bessel beams", Opt. Express **16**, 15733-15740 (2008).

[3] S. Akturk, B. Zhou, M. Franco, A. Couairon, A. Mysyrowicz, "Generation of long plasma channels in air by focusing ultrashort laser pulses with an axicon", Opt. Commun. **282**, 129-134 (2009).

[4] P. Polynkin, M. Kolesik, J. Moloney, "Extended filamentation with temporally chirped femtosecond Bessel-Gauss beams in air", Opt. Express **17**, 575-584 (2009).

[5] P. Polynkin, M. Kolesik, J. Moloney, G. Siviloglou, D. Christodoulides, "Curved plasma channel generation using ultraintense Airy beams", Science **324**, 229-232 (2009).

[6] I. J. Sola et al., "High power vortex generation with volume phase holograms and non-linear experiments in gases", Appl. Phys. B **91**, 115-118 (2008).

[7] P. Polynkin, C. Ament, J. V. Moloney, "Self-focusing of ultraintense femtosecond optical vortices in air", Phys. Rev. Lett. **111**, 023901 (2013).

[8] M. Chateauneuf, S. Payeur, J. Dubuis, J.-C. Kieffer, "Microwave guiding in air by a cylindrical filament array waveguide", Appl. Phys. Lett. **92**, 091104 (2008).

[9] A. Alshershby, Z. Q. Hao, J. Q. Lin, "Guiding microwave radiation using laser-induced filaments: the hollow conducting waveguide concept", J. Phys. D **45**, 265401 (2012).

[10] M. S. Soskin, M. V. Vasnetsov, "Singular optics", Prog. Opt. **42**, 219-276 (2001).

[11] B. C. Stuart, M. D. Feit, S. Herman, A. M. Rubenchik, B. W. Shore, M. D. Perry, "Nanosecond-to-femtosecond laser-induced breakdown in dielectrics", Phys. Rev. B **53**, 1749-1761 (1996).